Soil & Tillage Research 178 (2018) 150–158

Contents lists available at ScienceDirect

Soil & Tillage Research

journal homepage: www.elsevier.com/locate/still

Quantifying contributions of slaking and mechanical breakdown of soil aggregates to splash erosion for different soils from the Loess plateau of China

Hai Xiao[a,c], Gang Liu[a,b,*], Qiong Zhang[a], Zheng Fenli[a,b], Xunchang Zhang[d], Puling Liu[a,b], Jiaqiong Zhang[a,b], Feinan Hu[a,b], Mohamed A. M. Abd Elbasit[e]

[a] *State Key Laboratory of Soil Erosion and Dryland Farming on the Loess Plateau, Institute of Soil and Water Conservation, Northwest A&F University, Yangling 712100, People's Republic of China*

[b] *Institute of Soil and Water Conservation of Chinese Academy of Sciences and Ministry of Water Resources, Yangling 712100, People's Republic of China*

[c] *Key Laboratory of Geological Hazards on Three Gorges Reservoir Area (China Three Gorges University), Ministry of Education, Yichang 443002, People's Republic of China*

[d] *USDA-ARS, Grazinglands Research Lab., 7207 W. Cheyenne St., El Reno, OK 73036, USA*

[e] *Agricultural Research Council, Institute for Soil, Climate & Water, Private Bag X79, Pretoria 0001, South Africa*

ARTICLE INFO

Keywords:
Aggregate disintegration
Slaking
Mechanical breakdown
Rainfall kinetic energy
Soil texture

ABSTRACT

The information of aggregate disintegration mechanisms during splash erosion is scant. This study was conducted to quantify contributions of the mechanisms of aggregate disintegration to splash erosion. Six soils with five soil textures were used. Soil aggregate stability was determined by the Le Bissonnais (LB) method. Deionized water was used to simulate the combined effect of slaking and mechanical disaggregation, while ethanol was used to estimate the sole contribution of the mechanical breakdown. Simulated rainfall with intensity of 60 mm h^{-1} was applied at five fall heights (0.5 m, 1 m, 1.5 m, 2 m and 2.5 m) to achieve different levels of rainfall kinetic energy. The results indicated that slaking caused the most severe aggregate breakdown, and followed by mechanical breakdown, while chemical dispersion in slow wetting with deionized water was the weakest breakdown mechanism. The splash erosion rates due to the effects of slaking and mechanical breakdown increased with an increase in rainfall kinetic energy. The contributions of the slaking (mechanical breakdown) to splash erosion decreased (increased) as rainfall kinetic energy increased. The contribution of mechanical breakdown had a power function relation with rainfall kinetic energy, and had the most significant correlation with *RSI* (relative slaking index)/*RMI* (relative mechanical breakdown index). A power and a linear function could be used to describe the relationships between the contributions of mechanical breakdown with rainfall kinetic energy and *RSI*/*RMI*, respectively, which could be used to estimate the contribution of mechanical breakdown. The results of this research would be helpful to improving the soil erosion prediction models.

1. Introduction

Slaking (caused by the compression of air entrapped inside aggregates during wetting), differential swelling of clays, mechanical dispersion due to the kinetic energy of raindrops and physicochemical dispersion are considered as four main mechanisms for soil aggregates disintegration (Le Bissonnais, 1996). Aggregate breakdown is of significant importance in the soil detachment for which it provides fine particles that are splashable by raindrops (Wuddivira et al., 2009) and transportable by raindrop-impacted sheet flow. Auerswald (1995) concluded that air entrapment by rapid wetting was the main cause of aggregate disintegration, while swelling and clay dispersion had minor or no effect on aggregate disintegration. It was demonstrated that swelling and clay dispersion had minor or no effect on aggregate disintegration by comparing between different moisture pretreatments and liquids (Almajmaie et al., 2017). Loch (1994) demonstrated that aggregate disintegration depended on the wetting rate (slaking) at which the initially dry aggregates are wetted, and was an energetically more important process than the impact of raindrops. Fajardo et al. (2016) showed that slaking occurred mainly during the initial few minutes under fast wetting condition by using an image recognition algorithm method. Han et al. (2016) confirmed the importance of slaking on soil disaggregation. Mechanical breakdown due to raindrop impact is another important soil aggregate breakdown mechanism

* Corresponding author at: No. 26, Xinong Road, Yangling, Shaanxi Province, 712100, PR China.
E-mail address: gliu@foxmail.com (G. Liu).

https://doi.org/10.1016/j.still.2017.12.026
Received 4 September 2017; Received in revised form 30 December 2017; Accepted 30 December 2017
Available online 13 January 2018
0167-1987/

Table 1
Basic physical and chemical property of experimental soils.

Soil	Sampling location	Clay/%	Slit/%	Sand/%	Soil organic matter/ g kg^{-1}	pH value (1:2.5)	Air dried soil moisture content/%	Water drop penetration time/s	Free-form Fe/ g/kg	Amorphous Fe/g/kg	Free-form Al/ g/kg	Amorphous Al/g/kg
Loam clay soil	Yangling	26.1	40.0	33.9	6.0	8.4	2.6	0.20	7.96	0.56	3.61	0.60
Clay loam soil	Changwu	20.9	33.1	46.1	10.1	8.2	3.3	0.24	5.98	0.41	1.50	0.61
Sandy loam soil 1	Ansai	10.6	18.9	70.5	4.1	8.8	1.1	0.19	4.94	0.33	2.37	0.15
Sandy loam soil 2	Jingbian	11.5	21.4	67.1	4.8	8.8	1.0	0.27	4.94	0.30	4.80	0.38
Silty clay loam	Wugong	16.2	48.2	35.6	20.9	8.6	2.9	0.64	6.95	0.53	2.97	0.68
Loamy sand	Shenmu	6.3	6.8	86.9	2.4	8.7	1.0	0.28	4.76	0.14	0.74	0.48

during water erosion. Zhou et al. (2013) highlighted the significant importance of mechanical breakdown on aggregates during water erosion by observing the process of soil aggregate breakdown for different levels of rainfall kinetic energy. The raindrop impact is the major mechanism responsible for aggregate breakdown in the absence of slaking when soil moisture is near field capacity (Almajmaie et al., 2017). Thus, the main mechanisms of soil aggregate breakdown during water erosion processes are both slaking by fast wetting and mechanical breakdown due to raindrop impact (Shi et al., 2012; Vaezi et al., 2017). However, the information on assessing the rates of contributions of slaking and mechanical breakdown to water erosion is scant. Therefore, a systematic approach to determine the contribution rates of slaking and mechanical breakdown to water erosion during rainfall simulations is desirable.

Soil aggregation or disaggregation plays an important role in many soil functions (De Gryze et al., 2005; Deviren Saygm et al., 2012). Many researchers have reached the consensus that the indicator of structural stability of soil aggregates (Six et al., 2000), referred as aggregate stability, is in close relation to soil erosion (Mbagwu and Auerswald, 1999; Valmis et al., 2005; Shi et al., 2010; Xiao et al., 2017a). The clay, organic matter and Fe/Al oxides act as cementing agents that promote the formation of aggregates and increase aggregate stability (Puget et al., 1995; Le Bissonnais & Arrouays, 1997; Barthès et al. 2008; An et al., 2013).

The splash erosion due to raindrop impact increases with the breakdown of aggregates (Ma et al., 2014). The stability of topsoil aggregate is considered as a good indicator for both interrill (Barthès and Roose, 2002; Cantón et al., 2009; Shi et al., 2010) and rill erodibility (Wang et al., 2012). In addition, several researchers tried to use the aggregate stability, e.g. percolation stability (*PS*, an index of soil aggregate stability based on the amount of water percolated through a column of dry soil aggregates) (Mbagwu and Auerswald, 1999), instability index (β, an index of soil aggregate stability based on the mass of air-dry aggregates retained on the sieve after pre-soaked for 3 min immersion in water and 4 min oscillation) (Valmis et al.,2005; Dimoyiannis et al., 2006), for describing interrill erosion. The indexes of *PS* and β mainly reflect the fast wetting effect; however, the mechanisms primarily responsible for aggregate breakdown during water erosion processes include both slaking by fast wetting and mechanical breakdown due to raindrop impact (Shi et al., 2012). The aggregate stability index (A_s), which reflects the slaking by fast wetting and mechanical breakdown due to raindrop impact effects, was applied to replace interrill erodibility K_i (Yan et al., 2008; Shi et al., 2010) and rill erodibility factor K_r (Wang et al., 2012) in the erosion equation of the Water Erosion Prediction Project (WEPP) model. The index A_s is calculated by: $A_s = RSI \times RMI$, here *RSI* and *RMI* are relative slaking index and relative mechanical breakdown index, reflecting the susceptibility to slaking and mechanical breakdown, respectively.

Therefore, this study was conducted to quantify the contribution of the mechanisms of aggregate disintegration to splash erosion. The purposes of this study were (i) to analyze the factors affecting the contributions of slaking and mechanical breakdown to splash erosion; and (ii) to establish and verify the prediction equations for partitioning slaking and mechanical breakdown.

2. Materials and methods

2.1. Soils

Six soils with five soil textures (International System) were collected from Yangling (34°17′56″ N, 108°03′27″ E, loam clay soil), Changwu (35°13′57″ N, 107°41′20″ E, clay loam soil), Ansai (36°55′22″ N, 108°51′28″ E, sandy loam soil 1), Jingbian (37°22′55″ N, 108°49′55″ E, sandy loam soil 2), Wugong (34°25′27″ N, 108°04′22″ E, silty clay loam) and Shenmu (38°47′37″ N, 110°22′03″ E, loamy sand) in Shaanxi province, China, respectively. Soil samples collected from the uppermost 30-cm layer and transported to the State Key Laboratory of Soil Erosion and Dryland Farming on the Loess Plateau in Yangling, China. The soil samples were air-dried and gently sieved through a 5-mm sieve to remove the impurities such as roots and gravels in the soils. A Malvern Mastersizer 2000 laser diffraction device (Malvern Instruments Ltd., UK), the Rex Electric Chemical PHS-3E precision acidity meter (Shanghai Precision Scientific Instrument Co., Ltd, China) and the potassium dichromate oxidation-external heating method (Liu, 1996) were used to analyze soil particle size distribution, pH value and soil organic matter, respectively. The persistence of water repellency was measured using the water drop penetration time (WDPT) test (Obia et al., 2017). The free-form Fe/Al oxide and amorphous Fe/Al oxide were extracted using the dithionite-citrate-bicarbonate (DCB) method and the ammonium oxalate method (Li, 1997), respectively, and Fe and Al contents were determined with an ICP analyzer (Vista-MPX, Varian, Inc., Palo Alto, CA, USA). Some physicochemical properties of the soils used in this study are given in Table 1.

2.2. Experimental rainfall device

A needle type rainfall device was used to simulate artificial rainfall. The rainfall device consists of three parts (Fig.1): rainfall liquid supply apparatus, raindrop generator and support frame. The support frame is a 1.7 m long steel bar with a steel disk at bottom for stabilization. The liquid supply apparatus was placed on the top of the frame, and the raindrop generator could be adjusted to any height on the frame. The liquid supply apparatus was a plastic bucket connected with a plastic tube on the side of the plastic bucket. A switch was installed on the plastic tube to control flow rate. The outlet of the plastic tube was placed inside the drop generator. The drop generator was a steel cylinder with an open top (20 cm in diameter). Thirty-nine syringe needles with 0.6 mm in diameter were evenly installed at the bottom of the cylinder. Three outflow tubes were installed on the side of the cylinder at different heights to control the hydraulic head.

A slightly modified splash pan that was similar to that used by Ma et al. (2014) was used. The splash pan, made of galvanized iron sheet, consisted of collect area and test area. The collector was an inverted truncated cone (30 cm in height, 30-cm diameter on top, and 10-cm diameter on bottom). A cylinder with a 10-cm diameter and a 10-cm height was used as a tester and centered in the middle of the bottom of the collector. A piece of galvanized iron sheet was welded obliquely and sealed with solid glue between the collector and tester. An outlet was connected to the collector at the lowest point to collect material splashed out of the test area during rainfall simulation.

2.3. Experimental rainfall experiments

The drop former apparatus was set at a designed height before preparing the splash pan. Water content of the air-dried soil was determined and used to calculate the amount of the soil needed to obtain the representative bulk density values of the cultivated horizons for different soils. The bottom of the test cylinder was perforated and covered with an 8-cm layer of 1–2 cm pebble to facilitate drainage of percolating water. The predetermined amount of the air-dried soil was packed over the pebble, separated with a filter paper. The packed soil was about 2 cm thick. A piece of plastic plate was applied to smooth the surface of the packed soil gently to avoid aggregate breakdown during packing. The splash pan was placed in the center of the collector and

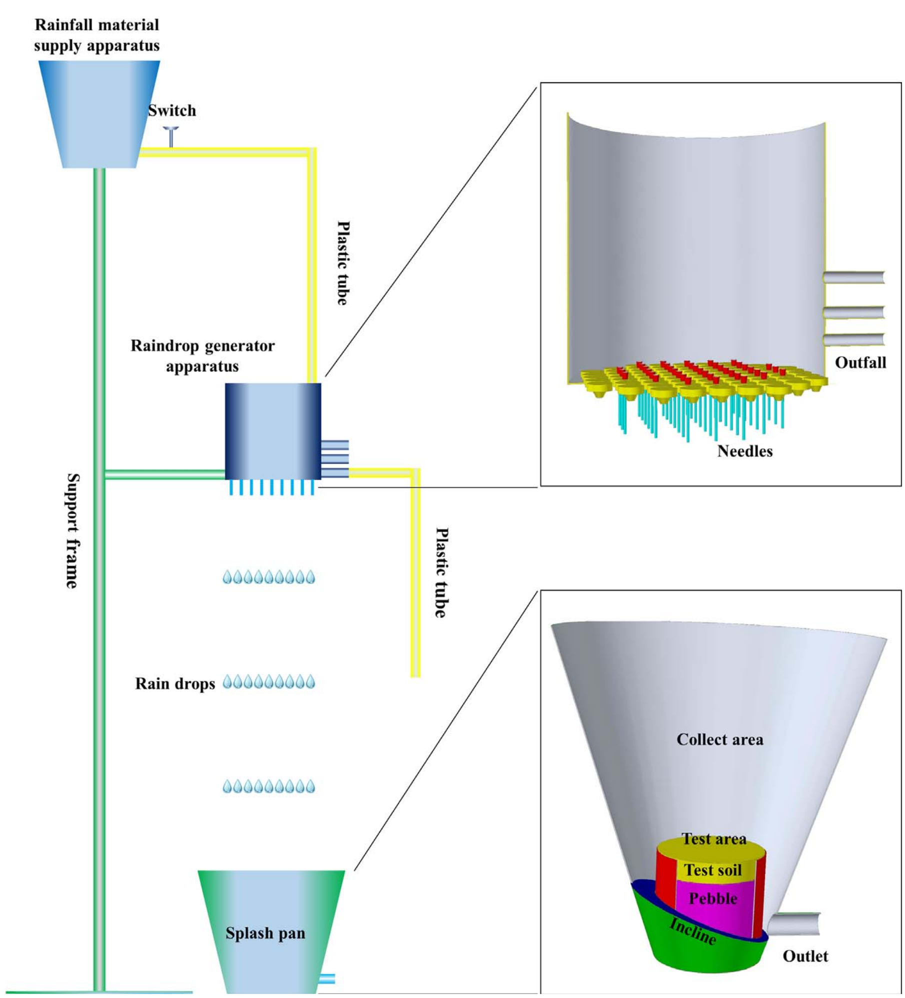

Fig. 1. Schematic representation of the experiment device.

covered with a rain shelter during the calibration of rainfall intensity. The rainfall intensity was controlled by using different constant heads. A constant hydraulic head was maintained in the rain maker during the rainfall simulations. The run with deionized water was terminated when water ponding appeared on the soil surface. It was about 10–20 min for loam clay soil, clay loam soil, sandy loam soil 1, sandy loam soil 2 and silty clay loam, and 20–30 min for loamy sand. For comparison, the duration of the ethanol run was set to the corresponding time of the deionized water run because ponding was never formed in the ethanol run. The splashed material was washed out with an extra injector of 50-ml volume and collected in a series of 100-ml beakers in an interval of 3 min throughout the test. The collected material was dried and weighed to an accuracy of 0.1 mg.

As mentioned above, the main soil aggregate breakdown mechanisms were slaking and mechanical breakdown by external force. The ethanol was used to minimize the effect of slaking due to the modification of surface tension, viscosity and contact angle (Merzouk and Blake, 1991; Le Bissonnais, 1996). The deionized water was used to simulate the effects of both slaking and mechanical breakdown during rainfall. A representative rainfall intensity of 60 mm h^{-1} was selected based on the natural maximum rainfall intensity occurring in a 10-min period in the Loess Plateau. In order to achieve different levels of drop kinetic energy and control the same wetting rate (slaking), experimental runs with the same rainfall intensity with five fall heights (0.5 m, 1 m, 1.5 m, 2 m and 2.5 m) were conducted. Each treatment replicated twice.

2.4. Measurement

The weight of ten rain drops and the corresponding time for each needle was measured with four replications after calibrating rainfall intensity to determine rainfall kinetic energy for different fall heights. The experiments were conducted at temperature of 20 ± 0.5 °C and standard atmospheric pressure. The drop was treated as spherical, and the drop diameter can be calculated as:

$$d = \sqrt[3]{\frac{6m}{\pi\rho_s}} \tag{1}$$

where d is the drop diameter (m); m is the measured mass of one raindrop (kg); ρ_s is the drop density (kg m^{-3}). The measured values of ρ_s were 998.0 and 809.9 for deionized water and ethanol, respectively. The terminal velocities under natural rainfall conditions are obtained when the velocity reaches its maximumas it falls through air. The terminal velocity (V) is reached when the raindrop weight (W) is exactly balanced by the upward buoyancy force (F_b) and drag force (D) ($W = F_b + D$).

$$W = mg = \rho_s Rg \tag{2}$$

$$F_b = \rho gR \tag{3}$$

$$D = \frac{1}{2}C_d\rho V^2 A = \frac{1}{8}\pi C_d\rho V^2 d^2 \tag{4}$$

$$V = \sqrt{\frac{4gd}{3C_d}(\frac{\rho_s}{\rho} - 1)} \tag{5}$$

where R is the volume of raindrop (m^3); g is the gravitational acceleration, 9.81 m s^{-2}; ρ is the density of air (kg m^{-3}), 1.29; C_d is the drag coefficient (C_d = 0.43 when the object is a sphere (Sha, 1956) and A is the projected area of the raindrop (m^2).

Since the raindrop velocity did not reach the terminal velocity for such short fall distances, the actual velocity was calculated using Eq. (6) (Hu et al., 2016):

$$v_a = V\sqrt{1-e^{-\frac{2g}{V^2}H}} \tag{6}$$

where v_a is the actual velocity (m s^{-1}) and H is the fall height (m). The individual raindrop kinetic energy can be calculated based on the theorem of kinetic energy using Eq. (8):

$$e_i = \frac{1}{2}m_i v_{ai}^2 \tag{7}$$

where e_i is the individual raindrop kinetic energy (J); m_i is the mass of raindrop i (kg); v_{ai} is the actual fall velocity of raindrop i (m s^{-1}). Salles et al. (2002) reviewed the literature about rain kinetic energy, and concluded that the time-specific rainfall kinetic energy expressed as the rain kinetic energy expended per unit area and per unit time was more appropriate than volume-specific rainfall kinetic energy when raindrop diameter and velocity were measured. Thus, the time-specific rainfall kinetic energy, i.e. the total raindrops' kinetic energy expended per unit area and per unit time was calculated as:

$$KE = \frac{\sum_{i=1}^{n=39} N_i e_i}{A_d} = \frac{\sum_{i=1}^{n=39} 36000/T_i e_i}{A_d} \tag{8}$$

where KE is the rainfall kinetic energy (J m^{-2} h^{-1}); N_i is the calculated raindrop number in one hour; T_i is the measured time for 10 raindrops for needle i (s); A_d is the raindrop impact area (m^2). Some raindrop parameters and the related rainfall kinetic energy for deionized water and ethanol tests are shown in Table 2.

The splash erosion rate was the material splashed out of the test area per unit area per unit time, which can be calculated using Eq. (13):

$$J_s = \frac{S}{A_s z} \tag{9}$$

where J_s is the splash erosion rate (g m^{-2} min^{-1}); S is the mass of the splashed material (g); A_s is the test area (m^2); z is the rainfall duration (min).

2.5. Measurement of aggregate stability

Soil aggregate stability was measured under different breakdown mechanisms: fast wetting (FW), slow wetting (SW), and mechanical breakdown by stirring pre-wetted aggregates (WS) using the Le Bissonnais (1996) method that combined four steps. (1) Three subsamples, 5 g each of air-dried aggregates of 3–5 mm in diameter were taken using a small spoon, was obtained by dry sieving and oven-dried at 40 °C for 24 h. (2) Pretreatment: For FW treatment, aggregates were gently immersed in distilled water for 10 min and the water was vacuumed off; For SW treatment, aggregates were placed on a filter-paper for 30 min, and subjected to a tension of 0.3 kPa; For WS treatment, aggregates were immersed in ethanol (95% in mass) for 10 min and transferred to a 500 ml flask with 200 cm^3 deionized water, corked and agitated up and down 20 times for 1 min, and then allowed to settle for 30 min. (3) The corresponding aggregates were transferred to a 0.05 mm sieve immersed in ethanol (95% in mass) and gently moved up

Table 2
Raindrop parameters and related rainfall kinetic energy for different fall heights for the deionized water and ethanol simulated rainfall tests.

Liquid	Fall height/m	Time for 10 raindrops/s	Weight of 10 raindrops/g	Mean raindrop diameter/mm	Rainfall kinetic energy/J m^{-2} h^{-1}
Deionized water	0.5	9.91	0.0945	2.62	57.23
	1.0	9.91	0.0947	2.63	196.61
	1.5	9.91	0.0945	2.62	381.03
	2.0	9.92	0.0948	2.63	596.94
	2.5	9.91	0.0945	2.62	796.22
Ethanol	0.5	6.45	0.0354	2.03	48.06
	1.0	6.23	0.0357	2.03	157.94
	1.5	6.34	0.0355	2.03	277.29
	2.0	6.29	0.0356	2.03	401.32
	2.5	6.33	0.0356	2.03	506.26

and down (2 cm in height) 20 times by hand. (4) The remaining aggregates on the 0.05 mm sieve were collected and measured for their size distribution by dry sieving through 3.0, 2.0, 1.0, 0.5, 0.2, 0.1 and 0.05 mm pore openings after drying in an oven at 40 °C for 48 h. Each treatment was replicated 3 times.

Aggregate stability for each sample was expressed in terms of the mean weight diameter (*MWD*) weighted over different size classes:

$$MWD = \sum_{i=1}^{n} \overline{x_i} w_i \tag{10}$$

where w_i is the weight fraction of aggregates in size class i with an average diameter $\overline{x_i}$. The relative slaking index (*RSI*) and the relative mechanical breakdown index (*RMI*) were used to determine the resistance to slaking and the mechanical breakdown of the soils (Zhang and Horn, 2001):

$$RSI = \frac{MWD_{sw} - MWD_{fw}}{MWD_{sw}} \tag{11}$$

$$RMI = \frac{MWD_{sw} - MWD_{ws}}{MWD_{sw}} \tag{12}$$

where MWD_{fw}, MWD_{ws}, and MWD_{sw} are the mean weight diameter obtained by the FW, WS, and SW treatments, respectively. The larger is the RSI or RMI, the more susceptible are the aggregates to slaking or mechanical breakdown, respectively (Zhang and Horn, 2001).

2.6. Statistics and data analysis

All statistical analyses were performed using Excel 2016 and SPSS 21.0 (SPSS Inc., Chicago, IL, USA). One-way analysis of variance (ANOVA) with a least significant difference (LSD) test was used to evaluate the differences of dependent variables (soil aggregate stability indexes) among different soils. Pearson correlation analysis was used to examine the relationships between dependent variables (i.e., soil aggregate stability indexes and the average contribution of mechanical breakdown) with influencing factors (i.e., particle size distribution and soil organic matter). Differences at the $P < 0.05$ level were considered to be significant. The Nash–Sutcliffe efficiency index (*NSE*), the normalized root mean square error (*NRMSE*), the average relative error (*AVE*) and the coefficient of determination (R^2) were used as indicators of model efficiency in this study (Moriasi et al., 2007).

$$NSE = 1 - \frac{\sum_{i=1}^{n} (X_{o,i} - X_{p,i})^2}{\sum_{i=1}^{n} (X_{o,i} - X_{o,avg})^2} \tag{13}$$

$$NRMSE = \frac{\sqrt{\frac{\sum_{i=1}^{n} (X_{o,i} - X_{p,i})^2}{n}}}{X_{o,avg}} \tag{14}$$

$$AVE = \frac{1}{N} \sum_{i=1}^{n} (\frac{X_{o,i} - X_{p,i}}{X_{o,i}}) \tag{15}$$

where $X_{o,i}$ is the observed value for i; $X_{p,\ i}$ is the predicted value for i; $X_{o,avg}$ is the mean observation value. NSE ranges between $-\infty$ and 1.0 (1 inclusive), with NSE = 1 being the optimal value. Values between 0.7 and 1.0 are generally viewed as good performance, values between 0.4 and 0.7 as satisfactory; whereas values less than 0.4 indicate unacceptable performance (Wu et al., 2016).

3. Results

3.1. General soil properties

Basic physicochemical properties of selected soils are summarized in Table 1. The soils used in this study were alkaline with pH values ranging from 8.2 to 8.8. The clay, silt, and sand contents of the soils ranged from 6.3% to 26.1%, from 6.8% to 48.2%, and from 33.9% to 86.9%, respectively. The organic matter contents of the soils were lower, with most of them being less than 20 g kg^{-1}. The soils were classified as not water-repellent type because the water drop penetration time was less than 5 s (Doerr et al., 2000). The contents of free-form and amorphous Fe ranged from 4.76 to 7.96 g kg^{-1} and from 0.14 to 0.56 g kg^{-1}, respectively. The contents of free-form and amorphous Al ranged from 0.74 to 4.80 g kg^{-1} and from 0.15 to 0.68 g kg^{-1}. The contents of Fe/Al (hydr) oxides in these soils were generally less than those in subtropical and tropical soils (Barthès et al., 2008; Zhao et al., 2017).

Table 3
Soil aggregate stability indexes measured by the Le Bissonnais (LB) method in this study.

Soil	MWD_{fw}/mm	MWD_{ws}/mm	MWD_{sw}/mm	*RSI*	*RMI*
Loam clay soil	0.43 a	2.11 a	2.65 a	0.84 a	0.20 f
Clay loam soil	0.32 b	1.35 b	1.93 b	0.83 a	0.30 e
Sandy loam soil 1	0.10 e	0.17 d	0.43 e	0.76 b	0.61 b
Sandy loam soil 2	0.10 e	0.18 d	0.39 f	0.75 b	0.54 c
Silty clay loam	0.27 c	0.95 c	1.68 c	0.84 a	0.43 d
Loamy sand	0.14 d	0.18 d	0.59 d	0.76 b	0.69 a

MWD_{fw}, MWD_{ws} and MWD_{sw} denote the mean weight diameters obtained after the fast-wetting (*FW*), pre-wetting and stirring (*WS*) and slow wetting (*SW*), respectively; *RSI* and *RMI* denote relative slaking index and relative mechanical breakdown index, respectively. Values followed by different letters in the same column indicate significant differences at the 0.05 level.

3.2. Aggregate stability indexes

The aggregate stability indexes for the six soils calculated by Eqs. (10)–(12) are shown in Table 3. The MWD_{fw}, MWD_{ws} and MWD_{sw} ranged from 0.10 to 0.43, from 0.17 to 2.11, and from 0.39 to 2.65, respectively. Significant differences existed among five soil textures for MWD_{fw} and among six soils for MWD_{sw}. Significant differences among loam clay soil, clay loam soil and silty clay loam were detected for MWD_{ws}, while no significant differences among sandy loam soil 1, sandy loam soil 2 and loamy sand were found. Generally, the *MWD* values decreased in the order of loam clay soil > clay loam soil > silty clay loam > loamy sand > sandy loam soil 1 and sandy loam soil 2. Pearson correlation indicated MWD_{fw}, MWD_{ws} and MWD_{sw} had significant positive correlations with clay ($P < 0.01$) and negative correlations with sand ($P < 0.05$), while no significant positive correlation with organic matter ($P > 0.05$) (Table 4). MWD_{fw}, MWD_{ws} *and* MWD_{sw} also demonstrated significant positive correlations with free-from Fe ($P < 0.01$) content, while no significant positive correlations with other Fe/Al (hydr) oxide contents ($P > 0.05$) except for a significant positive correlation between MWD_{sw} and amorphous Fe ($P < 0.05$) (Table 4). The aggregate stability values increased in the order of $MWD_{fw} < MWD_{ws} < MWD_{sw}$ for the three treatments for the six soils.

The *RSI* of the loam clay soil, silty clay loam and clay loam soil showed no significant differences with each other, and so did for sandy loam soil 1, sandy loam soil 2 and loamy sand. However, the *RSI* values of the former three soils were significantly lower than those of the latter three soils. The *RMI* showed significant differences among six soils and followed the order of loam clay soil < clay loam soil < silty clay loam < sandy loam soil 2 < sandy loam soil 1 < loamy sand. The soil aggregates of loam clay soil, silty clay loam and clay loam showed greater susceptibility to slaking than those of sandy loam soil 1, sandy loam soil 2 and loamy sand. The loamy sand was most susceptible to mechanical breakdown, while loam clay soil was the least susceptible to mechanical breakdown. Pearson correlations indicated that *RSI* was positively correlated with clay ($P < 0.05$) and negatively with sand ($P < 0.01$), while it had no significant positive correlation with organic matter ($P > 0.05$). Pearson correlation analysis also showed that

Table 4
Pearson correlation coefficients for the relationship between soil aggregate stability indexes and soil properties.

Soil aggregate stability indexes	Clay	Slit	Sand	SOM	Free-form Fe	Amorphous Fe	Free-form Al	Amorphous Al
MWDfw	0.935[b]	0.741	−0.845[a]	0.376	0.923[b]	0.786	0.031	0.755
MWDws	0.968[b]	0.732	−0.850[a]	0.308	0.921[b]	0.807	0.119	0.677
MWDsw	0.941[b]	0.782	−0.876[a]	0.430	0.936[b]	0.821[a]	0.049	0.759
RSI	0.853[a]	0.890[a]	−0.932[b]	0.693	0.902[a]	0.860[a]	−0.009	0.813[a]
RMI	−0.995[b]	−0.794	0.903[a]	−0.365	0.870[a]	0.854[a]	−0.280	−0.632

MWD_{fw}, MWD_{ws} and MWD_{sw} denote the mean weight diameters obtained after the fast-wetting (*FW*), pre-wetting and stirring (*WS*) and slow wetting (*SW*), respectively; *RSI* and *RMI* denote relative slaking index and relative mechanical breakdown index, respectively and SOM denote soil organic matter.
[a] Significant at 0.05 level of probability.
[b] Significant at 0.01 level of probability.

RMI was negatively correlated with clay ($P < 0.01$) and positively with sand ($P < 0.05$), while it had no significant negative correlation with organic matter ($P > 0.05$) (Table 4). *RSI* and *RMI* were not significantly correlated with Fe/Al (hydr) oxide contents ($P > 0.05$) but a significant positive correlation existed between *RSI* and amorphous Al ($P < 0.05$) (Table 4).

3.3. Splash rate at different kinetic energies of simulated rainfall

Fig. 2 shows that the splash erosion rates increased with the increasing of rainfall kinetic energy under both deionized water and ethanol tests. Power functions could describe the relation between splash erosion rates of the six soils and rainfall kinetic energy with the coefficient of determination (R^2) higher than 0.95 in both deionized water and ethanol tests (Table 5). The coefficient of power function can serve as an index of erosion severity with higher values reflecting higher soil erodibility (Xiao et al., 2017b). The coefficient of power function for deionized water and ethanol tests had no significant negative correlations with MWD_{fw}, MWD_{ws}, MWD_{sw}, and *RSI* ($P > 0.05$),

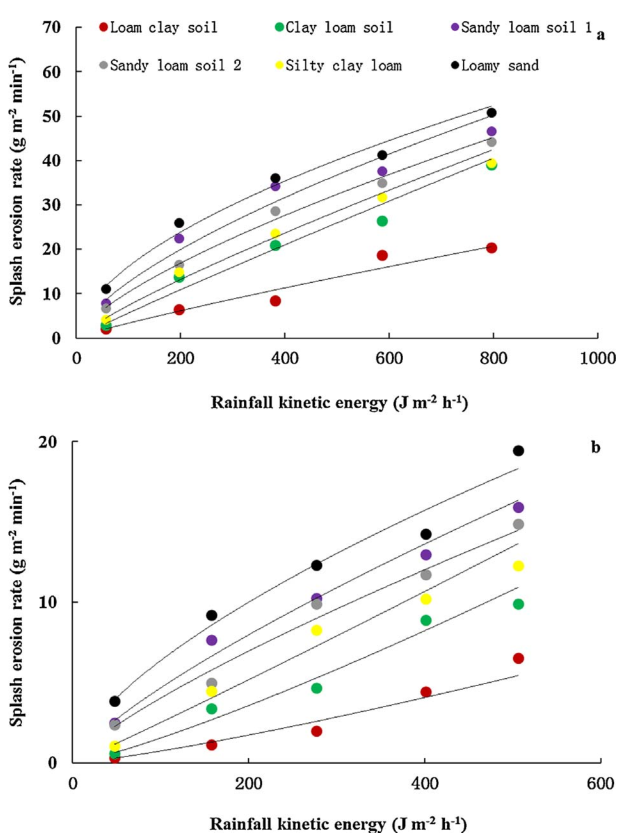

Fig. 2. Splash erosion rate at different rainfall kinetic energy for soil as determined with deionized water (a) and ethanol (b).

Table 5
Nonlinear regression between rainfall kinetic energy and splash erosion rate for deionized water and ethanol simulated rainfall tests.

Soil	Deionized water test	R^2	Ethanol test	R^2
Loam clay soil	$J_s = 0.060E^{0.873}$	0.972	$J_s = 0.003E^{1.232}$	0.975
Clay loam soil	$J_s = 0.071E^{0.949}$	0.975	$J_s = 0.006E^{1.206}$	0.982
Sandy loam soil 1	$J_s = 0.584E^{0.667}$	0.975	$J_s = 0.133E^{0.773}$	0.987
Sandy loam soil 2	$J_s = 0.390E^{0.711}$	0.997	$J_s = 0.107E^{0.788}$	0.984
Silty clay loam	$J_s = 0.150E^{0.844}$	0.990	$J_s = 0.021E^{1.044}$	0.988
Loamy sand	$J_s = 1.180E^{0.568}$	0.986	$J_s = 0.316E^{0.652}$	0.987

Where J_s is the splash rate ($g\,m^{-2}\,s^{-1}$) and E is the rainfall kinetic energy ($J\,m^{-2}\,h^{-1}$).

Table 6
Pearson correlation coefficients for the relationship between the coefficient of power function for deionized water and ethanol simulated rainfall tests and soil aggregate stability indexes.

The coefficient of power function	MWD_{fw}	MWD_{ws}	MWD_{sw}	*RSI*	*RMI*
Deionized water test	−0.687	−0.729	−0.721	−0.751	0.878[a]
Ethanol test	−0.686	−0.727	−0.722	−0.763	0.868[a]

MWD_{fw}, MWD_{ws} and MWD_{sw} denote the mean weight diameters obtained after the fast-wetting (*FW*), pre-wetting and stirring (*WS*) and slow wetting (*SW*), respectively; *RSI* and *RMI* denote relative slaking index and relative mechanical breakdown index, respectively.
[a] Significant at 0.05 level of probability.

while significant positive correlation with RMI ($P < 0.05$) existed (Table 6). The coefficients of loam clay soil, clay loam soil, silty clay loam, sandy loam soil 2, sandy loam soil 1 and loamy sand in the deionized water tests were 24.2, 11.9, 7.3, 3.7, 4.4 and 3.7 times larger than those in the ethanol tests. These results indicated that the soil was easier to be disaggregated in the deionized water test than in the ethanol test.

3.4. Effect of slaking and mechanical breakdown on splash erosion

As mentioned above, soil aggregates in deionized water rain suffered both slaking and mechanical breakdown while they were affected solely by mechanical breakdown in the ethanol rain. When the rainfall kinetic energy was the same, it can be assumed that the difference of splash erosion rates between the two tests was presumably attributed to slaking. Fig. 3(a) shows that the splash erosion rates caused by slaking and mechanical breakdown increased with the increase of rainfall kinetic energy for six soils. Meanwhile, the splash erosion rates of the soils caused by slaking are generally greater than those caused by mechanical breakdown, suggesting that slaking was more effective than mechanical breakdown in break up of soil aggregates. Fig. 3(b) shows, as rainfall kinetic energy increased, the contribution rate of slaking to splash erosion decreased while that of mechanical breakdown increased. The increased rainfall kinetic energy enhanced the mechanical breakdown by aggrandizing disruptive mechanical energy. Generally, the slaking contributed more than 50% when rainfall kinetic energy

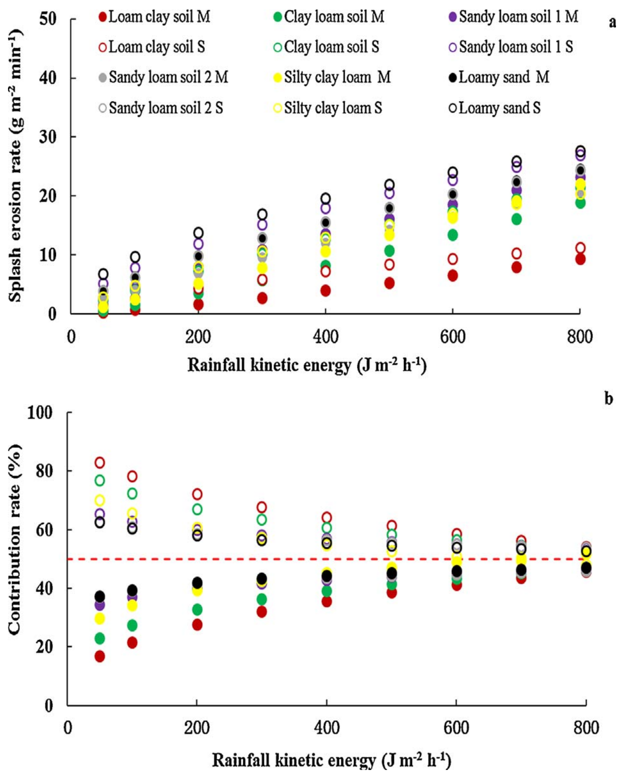

Fig. 3. Contributions of slaking and mechanical breakdown to splash erosion rates at different rainfall kinetic energy levels for six types of soil (a), and relative contributions between slaking and mechanical breakdown (b). (M = mechanical breakdown and S = slaking).

was between 50 and 800 J $m^{-2} h^{-1}$, especially for rainfall kinetic energy less than 300 J $m^{-2} h^{-1}$.

3.5. Factors affecting the contribution of slaking and mechanical breakdown to splash erosion

The contribution of mechanical breakdown was determined by the ratio of splash erosion by ethanol rainfall to deionized water rainfall for the same rainfall kinetic energy. The contribution of mechanical breakdown exhibited a power function relation with rainfall kinetic energy for each soil type. Pearson correlation analysis was conducted for analyzing the relationship between aggregate stability indexes the effect of aggregate stability indexes and soil properties related to the contribution of mechanical breakdown(Table 7). The average contribution of mechanical breakdown was calculated for the contributions of mechanical breakdown for rainfall kinetic energy 50, 100, 200, 300, 400, 500, 600, 700, 800 J $m^{-2} h^{-1}$ for each soil type. The average contributions of mechanical breakdown were significantly correlated with MWD_{fw}, MWD_{ws}, and clay at P = 0.05 and with *RSI/RMI* at P = 0.01, while they were significantly correlated with *RMI* and *RSI* × *RMI* at P = 0.05, and yet there were no significant correlations with *RSI*, silt, sand, SOM and Fe/Al (hydr) oxide contents. The *RSI/RMI* had the most significant correlation with the average contribution of

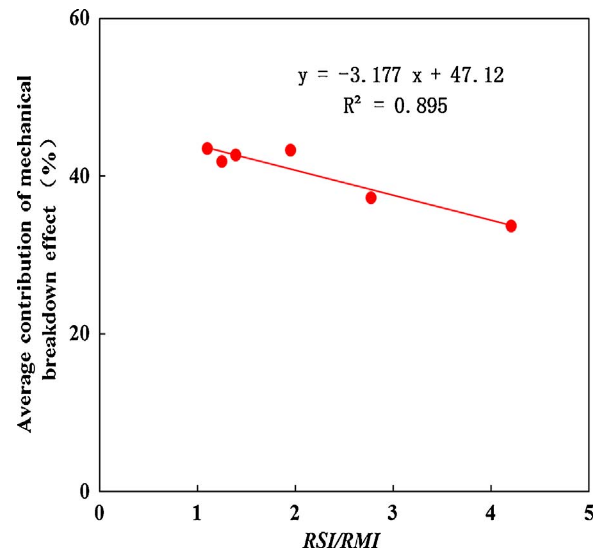

Fig. 4. Relationship between average contribution of mechanical breakdown and *RSI/RMI*. (*RSI* and *RMI* denote relative slaking index and relative mechanical breakdown index, respectively).

mechanical breakdown, and a linear function could describe their relationship with R^2 = 0.895 (Fig. 4), so *RSI/RMI* was selected to express the contribution of mechanical breakdown with a linear function. Since the corresponding contribution of slaking would obviously always exhibit results opposite to the contribution of mechanical breakdown, it is unnecessary to statistically analyze the factors affecting the contribution of slaking again.

3.6. Estimating the contribution of slaking and mechanical breakdown

To estimate the contribution of mechanical breakdown to splash erosion, an equation describing a power function with rainfall kinetic energy and a linear relation with *RSI/RMI* (c.f. Eq. (16)) was established by using the data of the loam clay soil, sandy loam soil 1 and silty clay loam soil. The contribution of slaking was estimated by subtracting the contribution of mechanical breakdown from 100%.

$$\mathrm{MC} = 17.601\mathrm{KE}^{0.172} - 3.153\frac{RSI}{RMI} \quad R^2 = 0.889 \tag{16}$$

$$SC = 100 - MC \tag{17}$$

where *MC* is the contribution of mechanical breakdown (%); *SC* is the contribution of slaking (%); *KE* is rainfall kinetic energy (J $m^{-2} h^{-1}$).

The remaining data of clay loam soil, sandy loam soil 2 and loamy sand were used for model efficiency validation (Fig. 5). The relationship between measured and estimated contribution of mechanical breakdown and slaking followed the 1:1 line, as shown in Fig. 5, with a R^2 of 0.799, *NSE* of 0.765, *NRMSE* of 0.082 and *AVE* of −0.017 for mechanical breakdown and 0.799, 0.765, 0.059 and 0.023, respectively, for slaking. This illustrates Eqs. (16) and (17) can explain 80.0% of the variance in the contributions of mechanical breakdown and slaking with small relative residuals of 8.3% and 6.0%, respectively, and can

Table 7
Pearson correlation coefficients for the relationship between aggregate stability indexes and soil properties related to the contribution of mechanical breakdown.

	MWD_{fw}	MWD_{ws}	*RSI*	*RMI*	*RSI* × *RMI*	*RSI/RMI*	Clay	Slit	Sand	SOM	Free-form Fe	Amorphous Fe	Free-form Al	Amorphous Al
AMC	−0.839[a]	−0.894[a]	−0.613	0.871[a]	0.863[a]	−0.936[b]	−0.894[a]	−0.431	0.611	0.105	−0.695	−0.593	−0.115	0.346

AMC denote the contribution of average mechanical breakdown; MWD_{fw}, MWD_{ws} and MWD_{sw} denote the mean weight diameters obtained after the fast-wetting (*FW*), pre-wetting and stirring (*WS*) and slow wetting (*SW*), respectively; *RSI* and *RMI* denote relative slaking index and relative mechanical breakdown index, respectively and SOM denote soil organic matter.
[a] Significant at 0.05 level of probability.
[b] Significant at 0.01 level of probability.

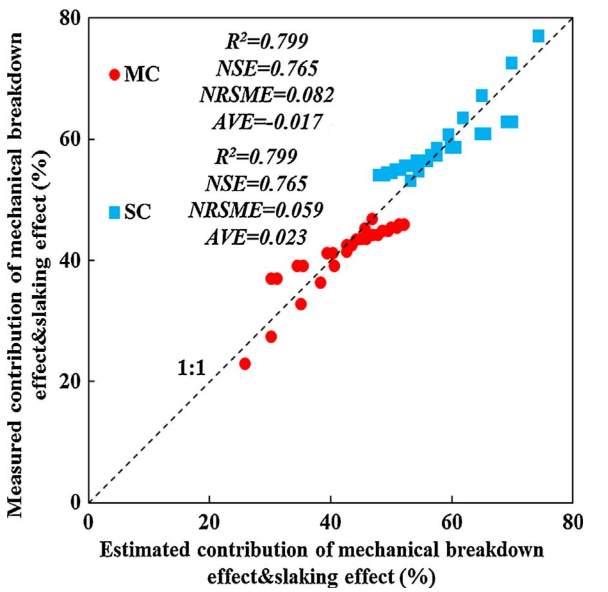

Fig. 5. Relationship between measured and estimated rate of contribution of mechanical breakdown and slaking for validating. (MC and SC denote contribution of mechanical breakdown and slaking, respectively).

predict the contributions of mechanical breakdown and slaking with average relative errors of −1.7% and 2.3%. The *NSE* values for Eqs. (16) and (17) were 0.766, indicating a good level of performance for these equations.

4. Discussion

Both clay and organic matter act as cementing agents that promote the formation of aggregates and increase aggregate stability (Puget et al., 1995; Le Bissonnais and Arrouays, 1997; An et al., 2013; Jozefaciuk and Czachor, 2014). The aggregate stability was significantly positively correlated with clay but not with organic matter (Table 4). Our results confirmed the previous findings by Le Bissonnais et al. (2007) that the increase in clay content could largely explain the increase in soil aggregate stability when organic C contents were low. In this study, slaking (FW) was the most effective aggregate breakdown mechanism followed by mechanical breakdown (WS), while chemical dispersion (SW) was the weakest breakdown mechanism for soil aggregate. This is in accordance with previous findings of other researchers who used the same experimental procedures (Yan et al., 2008; Shi et al., 2010; Algayer et al., 2014). The clay content has significant positive correlation with *RSI* and negative correlation with *RMI*, respectively (Table 4). This can be attributed to the inconformity increment of MWD_{fw}, MWD_{ws} and MWD_{sw} when the clay content increased (Table 3). Although Fe/Al (hydr) oxides are other major binding agents for aggregates (Barthès et al., 2008; Peng et al., 2015; Zhao et al., 2017), most of them showed no close relationship with aggregate stability except free-form Fe. This can be attributed to the low content of Fe/Al (hydr) oxide in the soils used in this study.

The power function relationship between splash erosion rate and rainfall kinetic energy is consistent with the conclusions of the previous research (Sharma et al., 1991; Hu et al., 2016). The negative relationship between soil erodibility and aggregate stability is consistent with the conclusions of the previous studies (Barthès and Roose, 2002; Nciizah and Wakindiki, 2015; Ding and Zhang, 2016). Higher aggregate stability can reduce erodibility due to the fact that the stable aggregates increase resistance to raindrop detachment (Ding and Zhang, 2016). The greater soil erodibility in the deionized water test than in the ethanol test may result from the difference in aggregate breakdown mechanisms. Soil aggregates in the deionized water test suffered from both slaking and mechanical breakdown due to rainfall kinetic impacts. But only mechanical breakdown was effective to disrupt soil aggregates in the ethanol test (Le Bissonnais, 1996; Legout et al., 2005).

The slaking contributed more than mechanical breakdown to disaggregation, which may be attributed to the air-dried soil used in this research. This result corroborated the findings that slaking rather than raindrop impact is the dominant mechanism for soil aggregate disintegration in dry soil (Han et al., 2016; Almajmaie et al., 2017). However, the force of raindrop impact plays a larger role in breaking aggregates when the initial moisture content is high (Lado et al., 2004). With an increase of the initial soil moisture, volume of the entrapped air decreases, resulting in lower compression forces acting on the aggregates during fast wetting (Vermang et al., 2009). In addition, slaking is also controlled by wetting rate, i.e. the faster the wetting rate the greater the slaking forces (Lado et al., 2004; Fan et al., 2008; Yan et al., 2010; Rodrigo et al., 2016).

The aggregate stability index (A_s) was used in some researches (Yan et al., 2008; Shi et al., 2010; Wang et al., 2012) basing on the assumption that slaking and mechanical breakdown has the same effect on soil erodibility. However, the results in our study indicated that their effects on aggregate disintegration depend on *RSI*/*RMI* and rainfall kinetic energy. Splash detachment is an important phenomenon and an initial step in erosion process (Van Dijk et al., 2002; Leguédois et al., 2005; Hu et al., 2016; Saedi et al., 2016), and it is a key process in interrill erosion because it produces detached soil particles for transport by the raindrop-impacted sheet flow (Legout et al., 2005; Dimoyiannis et al., 2006). Thus, an error may result when using A_s to calculate interrill erosion. Therefore, to improve the accuracy of an interrill erosion prediction model, different contribution rates of slaking and mechanical breakdown should be considered.

Eqs. (16) and (17) highlighted the importance of rainfall kinetic energy and *RSI*/*RMI* for aggregate disintegration mechanisms to splash erosion. However, they were obtained based on experiments using one rainfall intensity with air-dried soil. Hitherto, many research studies underlined the influence of the wetting rate and initial soil moisture on aggregate stability particularly on slaking (Mamedov et al., 2002; Shainberg et al., 2003; Rodrigo et al., 2016). To fully understand the aggregate destruction during erosion, a wider range of soil moisture contents under a wider rainfall conditions should be further investigated.

5. Conclusions

The contributions of slaking and mechanical breakdown to splash erosion were estimated by measuring the splash erosion under deionized water and ethanol test. Splash erosion rate increased with increases of rainfall kinetic energy, and a power function could effectively describe their relations with R^2 higher than 0.95 in both deionized water and ethanol tests. The contribution rates of slaking to the splash erosion rates decreased, whereas those of mechanical breakdown increased as rainfall kinetic energy increased. The effect of slaking and mechanical breakdown on aggregate disintegration also depends on *RSI*/*RMI*. An equation combining a power function with rainfall kinetic energy and a linear function with *RSI*/*RMI* was developed for estimating the contribution of mechanical breakdown to splash erosion. The validation showed the equation performed reasonably well.

Acknowledgments

The authors are grateful to the editors and the anonymous reviewers for their constructive comments that have considerably improved this paper. This research was jointly supported by the National Science Foundation of China (No. 41761144060), the National Key R&D Program of China (No. 2016YFE0202900), the International Partnership Program of Chinese Academy of Sciences (No.161461KYSB20170013), the National Key Technology Research and Development Program of the Ministry of Science and Technology of China (No. 2015BAC01B03-03), the Innovative Talents Promotion Plan in Shaanxi Province (No. 2017KJXX-83), the Key Laboratory Projects of Natural Science Foundation of Hubei Province of China (2016CFA085) and the open fund of Key Laboratory of Geological Hazards on Three Gorges Reservoir Area, Ministry of Education (China Three Gorges University) (Grant No. 2017KDZ10).

References

Almajmaie, A., Hardie, M., Acuna, T., Colin, B., 2017. Evaluation of methods for determining soil aggregate stability. Soil Tillage Res. 167, 39–45.

Algayer, B., Wang, B., Bourennane, H., Zheng, F.L., Duval, O., Li, G.F., Le Bissonnais, Y., Darboux, F., 2014. Aggregate stability of a crusted soil: differences between crust and sub-crust material, and consequences for interrill erodibility assessment: an example from the Loess plateau of China. Eur. J. Soil Sci. 65 (3), 1–11.

An, S.S., Darboux, F., Cheng, M., 2013. Revegetation as an efficient means of increasing soil aggregate stability on the Loess plateau (China). Geoderma 209–210, 75–85.

Auerswald, K., 1995. Percolation stability of aggregates from arable topsoils. Soil Sci. 159, 142–148.

Barthès, B., Roose, E., 2002. Aggregate stability as an indicator of soil susceptibility to runoff and erosion: validation at several levels. Catena 47, 133–149.

Barthès, B.G., Kouakoua, E., Larré-Larrouy, M.C., Razafimbelo, T.M., Luca, E.F.D., Azontonde, A., Neves, C.S.V.J., Freitas, P.L.D., Feller, C.L., 2008. Texture and sesquioxide effects on water-stable aggregates and organic matter in some tropical soils. Geoderma 143, 14–25.

Cantón, Y., Solé-Benet, A., Asensio, C., Chamizo, S., Puigdefábregas, J., 2009. Aggregate stability in range sandy loam soils relationships with runoff and erosion. Catena 77, 192–199.

De Gryze, S., Six, J., Brits, C., Merckx, R., 2005. A quantification of short-term macroaggregate dynamics: influences of wheat residue input and texture. Soil Biol. Biochem. 37 (1), 55–66.

Deviren Saygm, S., Cornelis, W.M., Erpul, G., Gabriels, D., 2012. Comparison of different aggregate stability approaches for loamy sand soils. Appl. Soil Ecol. 54, 1–6.

Dimoyiannis, D., Valmis, S., Danalatos, N.G., 2006. Interrill erosion on cultivated Greek soils: modeling sediment delivery. Earth Surf. Proc. Land 31, 940–949.

Ding, W.F., Zhang, X.C., 2016. An evaluation on using soil aggregate stability as the indicator of interrill erodibility. J. Mt. Sci. Engl. 13 (5), 831–843.

Doerr, S.H., Shakesby, R.A., Walsh, R.P.D., 2000. Soil water repellency: its causes, characteristics and hydro-geomorphological significance. Earth Sci. Rev. 51, 33–65.

Fajardo, M., Mcbratney, A.B., Field, D.J., Minasny, B., 2016. Soil slaking assessment using image recognition. Soil Tillage Res. 163, 119–129.

Fan, Y., Lei, T., Shainberg, I., Cai, Q., 2008. Wetting rate and rain depth effects on crust strength and micromorphology. Soil Sci. Soc. Am. J. 72, 1604–1610.

Han, Y.G., Fan, Y.T., Xin, Z.B., Wang, L., Cai, Q.G., Wang, X.Y., 2016. Effects of wetting rate and simulated rain duration on soil crust formation of red loam. Environ. Earth Sci. 75 (2), 149.

Hu, W., Zhen, F.L., Bian, F., 2016. The directional components of splash erosion at different raindrop kinetic energy in the Chinese Mollisol region. Soil Sci. Soc. Am. J. 80, 1329–1340.

Jozefaciuk, G., Czachor, H., 2014. Impact of organic matter, iron oxides, alumina, silica and drying on mechanical and water stability of artificial soil aggregates. assessment of new method to study water stability. Geoderma 221–222, 1–10.

Lado, M., Ben-Hur, M., Shainberg, I., 2004. Soil wetting and texture effects on aggregate stability, seal formation, and erosion. Soil Sci. Soc. Am. J. 68, 1992–1999.

Loch, R.J., 1994. Structure breakdown on wetting. Sealing, Rusting and Hard Setting Soils. Australian Soil Science Society Queensland Press, Brisbane.

Le Bissonnais, Y., 1996. Aggregate stability and assessment of soil crustability and erodibility: I. Theory and methodology. Eur. J. Soil Sci. 47, 425–437.

Le Bissonnais, Y., Arrouays, D., 1997. Aggregate stability and assessment of crustability and erodibility. II. Application to humic loamy soils with various organic carbon content. Eur. J. Soil Sci. 48, 39–48.

Le Bissonnais, Y., Blavet, D., De Noni, G., Laurent, J.Y., Asseline, J., Chenu, C., 2007. Erodibility of Mediterranean vineyard soils: relevant aggregate stability methods and significant soil variables. Eur. J. Soil Sci. 58, 188–195.

Legout, C., Leguédois, S., Le Bissonnais, Y., Malam Issa, O., 2005. Splash distance and size distributions for various soils. Geoderma 124, 279–292.

Leguédois, S., Planchon, O., Legout, C., Le Bissonnais, Y., 2005. Splash projection distance for aggregated soils: theory and experiment. Soil Sci. Soc. Am. J. 69, 30–37.

Li, X.Y., 1997. Soil Chemistry and Experimental Guidelines. China Agriculture Press, Beijing (in Chinese).

Liu, G.S., 1996. Soil Physical and Chemical Analysis and Description of Soil Profiles. Standards Press of China, Beijing (in Chinese).

Ma, R.M., Li, Z.X., Cai, C.F., Wang, J.G., 2014. The dynamic response of splash erosion to aggregate mechanical breakdown through rainfall simulation events in Ultisols (subtropical China). Catena 121, 279–287.

Mamedov, A.I., Shainberg, I., Levy, G.J., 2002. Wetting rate and sodicity effects on interrill erosion from semi-arid Israeli soils. Soil Tillage Res. 68, 121–132.

Mbagwu, J.S.C., Auerswald, K., 1999. Relationship of percolation stability of soil aggregates to land use, selected properties, structural indices and simulated rainfall erosion. Soil Tillage Res. 50, 197–206.

Merzouk, A., Blake, G.R., 1991. Indices for the estimation of interrill erodibility of Moroccan soils. Catena 18, 537–550.

Moriasi, D.N., Arnold, J.G., Van Liew, M.W., Bingner, R.L., Harmel, R.D., Veith, T.L., 2007. Model evaluation guidelines for systematic quantification of accuracy in watershed simulations. Trans. ASABE. 50 (3), 885–900.

Nciizah, A.D., Wakindiki, I.I.C., 2015. Physical indicators of soil erosion, aggregate stability and erodibility. Arch. Agron. Soil Sci. 61 (6), 827–842.

Obia, A., Børresen, T., Martinsen, V., Cornelissen, G., Mulder, J., 2017. Effect of biochar on crust formation, penetration resistance and hydraulic properties of two coarse-textured tropical soils. Soil Tillage Res. 170, 114–121.

Peng, X., Yan, X., Zhou, H., Zhang, Y.Z., Sun, H., 2015. Assessing the contributions of sesquioxides and soil organic matter to aggregation in an Ultisol under long-term fertilization. Soil Tillage Res. 146, 89–98.

Puget, P., Chenu, C., Balesdent, J., 1995. Total and young organic matter distributions in silty cultivated soils. Eur. J. Soil Sci. 46, 449–459.

Rodrigo, C.J., Iserloh, T., Lassu, T., Cerdà, A., Keestra, S.D., Prosdocimi, M., Brings, C., Marzen, M., Ramos, M.C., Senciales, J.M., Ruiz Sinoga, J.D., Seeger, M., Ries, J.B., 2016. Quantitative comparison of initial soil erosion processes and runoff generation in Spanish and German vineyards. Sci. Total Environ. 565, 1165–1174.

Saedi, T., Shorafa, M., Gorji, M., Moghadam, B.K., 2016. Indirect and direct effects of soil properties on soil splash erosion rate in calcareous soils of the central Zagross, Iran: a laboratory study. Geoderma 271, 1–9.

Salles, C., Poesen, J., Sempere-Torres, D., 2002. Kinetic energy of rain and its functional relationship with intensity. J. Hydrol. 257, 256–270.

Six, J., Elliott, E.T., Paustian, K., 2000. Soil macroaggregate turnover and microaggregate formation: a mechanism for C sequestration under no-tillage agriculture. Soil Biol. Biochem. 32 (14), 2099–2103.

Sha, Y.Q., 1956. Sediment Dynamics. China Industry Press, Beijing (in Chinese).

Shainberg, I., Mamedov, A.I., Levy, G.J., 2003. Role of wetting rate and rain energy in seal formation and erosion. Soil Sci. 168 (1), 54–62.

Shi, Z.H., Yan, F.L., LI, L., Li, Z.X., Cai, C.F., 2010. Interrill erosion from disturbed and undisturbed samples in relation to topsoil aggregate stability in red soils from subtropical China. Catena 81, 240–248.

Shi, Z.H., Yue, B.J., Wang, L., Fang, N.F., Wang, D., Wu, F.Z., 2012. Effects of mulch cover rate on interrill erosion processes and the size selectivity of eroded sediment on steep slopes. Soil Sci. Soc. Am. J. 77, 257–267.

Sharma, P.P., Gupta, S.C., Rawls, W.J., 1991. Soil detachment by single raindrops of varying kinetic energy. Soil Sci. Soc. Am. J. 55, 301–307.

Valmis, S., Dimoyiannis, D., Danalatos, N.G., 2005. Assessing interrill erosion rate from soil aggregate instability index, rainfall intensity and slope angle on cultivated soils in central Greece. Soil Tillage Res. 80, 139–147.

Vaezi, A.R., Ahmadi, M., Cerdà, A., 2017. Contribution of raindrop impact to the change of soil physical properties and water erosion under semi-arid rainfalls. Sci. Total Environ. 583, 382–392.

Van Dijk, A.I.J.M., Meesters, A.G.C.A., Bruijnzeel, L.A., 2002. Exponential distribution theory and the interpretation of splash detachment and transport experiments. Soil Sci. Soc. Am. J. 66, 1466–1474.

Vermang, J., Demeter, V., Cormeyer, W.M., Gabriels, D., 2009. Aggregate stability and erosion response to antecedent water content of a loess soil. Soil Sci. Soc. Am. J. 73 (3), 718–726.

Wang, J.G., Li, Z.X., Cai, C.F., Yang, W., Ma, R.M., Zhang, G.B., 2012. Predicting physical equations of soil detachment by simulated concentrated flow in Ultisols (subtropical China). Earth Surf. Proc. Land. 37, 633–641.

Wu, B., Wang, Z.L., Shen, N., Wang, S., 2016. Modelling sediment transport capacity of rill flow for loess sediments on steep slopes. Catena 147, 453–462.

Wuddivira, M.N., Stone, R.J., Ekwue, E.I., 2009. Clay, organic matter, and wetting effects on splash detachment and aggregate breakdown under intense rainfall. Soil Sci. Soc. Am. J. 73, 226–232.

Xiao, H., Liu, G., Liu, P.L., Zheng, F.L., Zhang, J.Q., Hu, F.N., 2017a. Developing equations to explore relationships between aggregate stability and erodibility in Ultisols of subtropical China. Catena 157, 279–285.

Xiao, H., Liu, G., Liu, P.L., Zheng, F.L., Zhang, J.Q., Hu, F.N., 2017b. Response of soil detachment rate to the hydraulic parameters of concentrated flow on steep loessial slopes in on the Loess Plateau of China. Hydrol. Process. 31, 2613–2621.

Yan, F.L., Shi, Z.H., Li, Z.X., Cai, C.F., 2008. Estimating interrill soil erosion from aggregate stability of Ultisols in subtropical China. Soil Tillage Res. 100, 34–41.

Yan, F.L., Shi, Z.H., Cai, C.F., Li, Z.X., 2010. Wetting rate and clay content effects on interrill erosion in Ultisols of southeastern China. Pedosphere 20 (1), 129–136.

Zhang, B., Horn, R., 2001. Mechanisms of aggregate stabilization in Ultisols from subtropical China. Geoderma 99, 123–145.

Zhao, J.S., Chen, S., Hu, R.G., Li, Y.Y., 2017. Aggregate stability and size distribution of red soils under different land uses integrally regulated by soil organic matter, and iron and aluminum oxides. Soil Tillage Res. 167, 73–79.

Zhou, H., Peng, X.H., Darboux, F., 2013. Effect of rainfall kinetic energy on crust formation and interrill erosion of an Ultisol in subtropical China. Vadose Zone J. 12, 1–9.